Quantum Liang Information Flow Probe of Causality across Critical Points

Roopayan Ghosh,[1,*] Bin Yi,[2,1] and Sougato Bose[1]
[1]Department of Physics and Astronomy, University College London, Gower Street, London WC1E 6BT, United Kingdom
[2]Institute of Fundamental and Frontier Sciences, University of Electronic Science and Technology of China, Chengdu 610051, China

(Received 3 May 2024; revised 15 November 2024; accepted 24 March 2025; published 18 April 2025; corrected 21 April 2025)

Investigating causation in the quantum domain is crucial. Despite numerous studies of correlations in quantum many-body systems, causation, which is very distinct from correlations, has hardly been studied. We address this by demonstrating the efficacy of the newly established causation measure, quantum Liang information flow, in quantifying causality across phase diagrams of quantum many-body systems. We focus on quantum criticality, which are highly nonclassical points. We extract causation behavior across a spectrum-wide critical point and a ground state second-order phase transition in both integrable and nonintegrable systems. Across criticality, each case exhibits distinct hallmarks, different from correlation measures. We also deduce that quantum causation qualitatively follows the quasiparticle picture of information propagation in integrable systems but exhibits enhanced quantum nonlocality near criticality. At times significantly larger than the spatial separation, it extracts additional features from the equilibrium wave function, leading to a peak just before the critical point for near boundary sites.

DOI: 10.1103/PhysRevLett.134.150202

Introduction—The study of dynamics of quantum many-body systems typically involves the time evolution of correlation functions and the spreading of entanglement [1–5]. Even the study of light cones, operator spreading [6–10], out-of-time-ordered correlators (OTOCs) [11–16], and quantum chaos measures [17,18] are essentially correlation studies. On the other hand, quantifying causation dynamics in the quantum realm, unlike classical theories, has been challenging [19]. In fact, the adage "correlation does not always imply causation" holds true even in the context of quantum mechanics, and the most commonly studied measures can, at best, detect a causal connection but not *quantify* the amount by which subsystems influence each other. We address this limitation in our Letter.

Model Hamiltonians of quantum chains provide the microcosm of quantum effects prevalent in our Universe. Hence, it is of paramount importance to find a measure of causation in these systems, which is easily measurable and can be appropriately connected to the physical intuition born from classical systems, yet demonstrating distinct quantum signatures. This has led to efforts in which quantum causation is extracted from quantum correlations, drawing inspiration from the Liang-Kleeman analysis used in classical systems [20–22], using von Neumann entropy [23]. The quantum version of Liang information flow (where the causal influence is defined as a property of interaction between two subsystems) offers distinct advantages over observable-based correlation measures that purportedly detect similar behavior. First, its use of information-theoretic tools makes it more universal. Second, it is intuitively connected to the classical picture and is easy to implement in experimental setups, as its simplest version requires only single-site measurements. However, its true test lies in whether it can properly quantify nonclassical phenomena. Critical regions in quantum many-body spin systems provide the perfect playground for this evaluation, which is where we focus our efforts.

In this Letter, we show that distinct signatures of quantum criticality are seen in quantum causation quantified by quantum Liang information flow. The key difference compared to just measuring entanglement entropy is that an intervention is applied, which allows us to measure quantum causation, not just correlations. To demonstrate, we conduct simulations of quench dynamics [24] using model Hamiltonians. Previous research has explored the time evolution of correlation functions for quenches across critical points in quantum many-body systems [25,26], leveraging nonanalyticities to detect phase transitions [27,28], but these do not demonstrate causality. Some studies involving OTOCs are also available in the literature [29–31], but their behavior frequently depends on the choice of operator due to possible conservation laws and they do not quantify causation. Our work suffers from no such drawbacks.

*Contact author: ucaprgh@ucl.ac.uk

Definitions—For density operator ρ, the von Neumann entropy $S(\rho)$ is defined as $S(\rho) = -\mathrm{Tr}[\rho \log \rho]$. Consider a system S with state ρ evolving under the unitary $U(t)$ generated by Hamiltonian H. Let the reduced density matrices of subsystems A, B, and AB be ρ_A, ρ_B, and ρ_{AB}, respectively. Following Ref. [23], the quantum Liang information flow is

$$T_{B\to A} = \frac{dS(\rho_A)}{dt} - \frac{dS(\rho_{A\not B})}{dt}, \tag{1}$$

where $\rho_{A\not B}$ is the density matrix of A with B frozen. While in Ref. [23] the derivative was used to denote rate of change of von Neumann entropy, for our purpose, the rhs can be considered to symbolically represent the Liang information flow at an infinitesimal time interval. If the system with frozen B evolves for time t, then the cumulative Liang information flow is

$$\mathbb{T}_d = S(\rho_A, t) - S(\rho_{A\not B}, t), \tag{2}$$

where d is the distance between A and B. This quantifies the *total* influence (Liang information flow) from B to A over time by tracking the change in A's entanglement with the system excluding B. Freezing a site effectively switches off certain Hamiltonian couplings, making Eq. (2) a measure of the "local quench" [32,33] effect on A. The setup is schematically illustrated in Fig. 1, see also Appendix A.

Localization transition in Aubry-Andre-Harper model—We first examine Liang information flow in the 1D Hamiltonian,

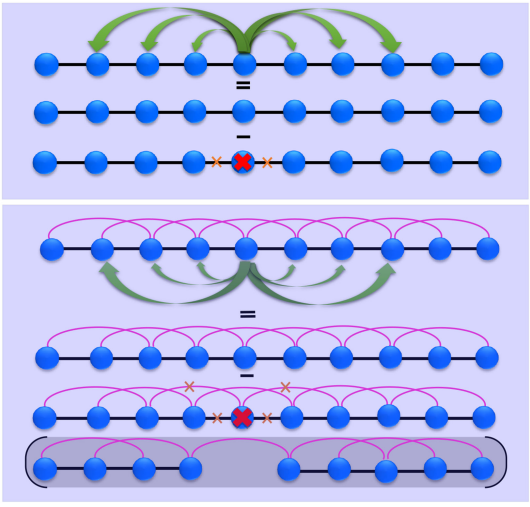

FIG. 1. Schematic of Liang information flow (green arrows) between a chosen site and others, computed by comparing an information flow in a normal lattice to one with a frozen site (cross). The top diagram shows nearest-neighbor coupling, while the bottom includes next-nearest-neighbor coupling.

$$H = \sum_{j=1}^{L-1}(\sigma_j^x\sigma_{j+1}^x + \sigma_j^y\sigma_{j+1}^y) + \frac{1}{2}\sum_{j=1}^{L}\mathcal{B}_j\sigma_j^z, \tag{3}$$

where $\sigma^{x,y,z}$ are Pauli-spin operators, $\mathcal{B}_j = \lambda\cos(2\pi\beta j)$, and $\beta = [(\sqrt{5}-1)/2]$, the inverse golden ratio. The system size L is chosen as a Fibonacci number to minimize finite-size effects [34]. This model undergoes a localization-delocalization transition at $\lambda = 2$ across its eigenspectrum [35].

In Fig. 2, we analyze the causal influence of a selected site across the transition using cumulative Liang information flow $\mathbb{T}_d$ between sites at distance d, averaged beyond the transient growth ($t \sim 10^2$). In Fig. 2(a), we observe that in the delocalized regime, there is equitable Liang information flow from the frozen site to others. This corroborates the unrestricted transport expected in this regime as a result of spatially extensive single-particle eigenfunctions. This indicates that, in large delocalized and ergodic systems, removing a few qubits, no matter their location in the chain, has no effect on dynamics. However, as λ nears the critical point, causation effects increase for nearby sites due to the restriction of information propagation beyond the localization length. Thus, local effects dominate a site's evolution. Since the phase transition spans the eigenspectrum, the initial state's energy has minimal impact. Therefore, our choice of the Néel state as the initial state gives similar qualitative results to other typical states (see Supplemental Material [36]).

In Fig. 2(b), we focus on two specific scenarios: (i) $d = 1$, representing a nearby site to the frozen site and (ii) $d = 15$, representing a site at a distance greater than the localization length in the localized regime. For the site at $d = 1$, we observe the anticipated behavior described in the preceding paragraph as λ increases. However, for distant sites, the causation flow becomes intriguing near

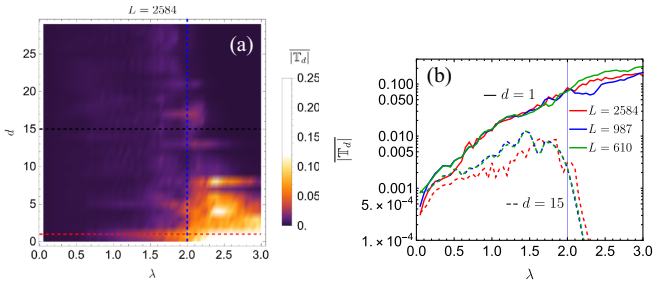

FIG. 2. Cumulative Liang information flow for the model in Eq. (4). (a) Late-time cumulative flow to a site d sites away from the frozen site, with $|T_d|$ averaged over $t \sim 10^2$ to smooth the plot. The blue dashed line marks the localization phase transition at $\lambda = 2$. (b) Cross section of (a) at the red dashed line, with similar data for other system sizes in different colors. The blue line marks the critical point. The frozen site position is the closest smaller Fibonacci number $+1$ to L, e.g., for $L = 2584$, $i = 1598$, to minimize finite-size effects.

criticality. For small λ, the behavior mirrors that of nearby sites, i.e., there is a gradual increase in cumulative Liang information flow with λ until approximately $\lambda \sim 1.5$. This is followed by a plateau before the expected sharp decline in the localized regime. This indicates a peak in causality occurs for an innocuous parameter, $\lambda < 2$, for distant sites. It also shows a slow drift toward $\lambda \sim 1.5$ for larger values of d, as seen in Fig. 2(a) from the faint violet regions. The larger causation values indicate an already inequitable flow of information between different sites in the said parameter regime. This, in turn, signifies traces of localization in the parts of the system acting as a herald to the onset of localization across the spectrum for $\lambda = 2$. A naive finite-size analysis in Fig. 2(b) suggests this effect is largely independent of system size. Furthermore, for $\lambda > 2$ exponentially localized wave functions result in exponentially small information leakage beyond the localization length, whose signature is given by a rapid but continuous decrease in Liang information flow with d.

Ground state phase transitions in Ising models—Next, we direct our focus to the anisotropic next-nearest-neighbor Ising (ANNNI) model with open boundary conditions (OBCs). This model includes a next-nearest-neighbor coupling, is nonintegrable, and lacks U(1) symmetry present in the previous example. In certain parameter regimes, the ground state of this model undergoes a ferromagnetic to paramagnetic Ising phase transition upon tuning the transverse magnetization strength. In the following analysis, we will investigate the influence of the middle site of the chain on other chosen sites across different parameter regimes. Note that choosing any other site in the bulk gives qualitatively same results.

The Hamiltonian of the ANNNI chain is given by

$$H_L = -\sum_{j}^{L-1} \sigma_j^z \sigma_{j+1}^z + \kappa \sum_{j}^{L-2} \sigma_j^z \sigma_{j+2}^z - \mathcal{B} \sum_{j}^{L} \sigma_j^x, \quad (4)$$

where κ represents the strength of the next-nearest-neighbor term and $\mathcal{B}$ is the magnitude of magnetic field applied along the transverse axis.

At fixed value of $0 \leq \kappa < 0.5$, the ground state of the ANNNI model undergoes quantum phase transition from the ferromagnetic to the paramagnetic phase when transverse field $\mathcal{B} > 0$ exceeds a critical value $\mathcal{B}_c$ [46–52], and the critical parameters κ_c and $\mathcal{B}_c$ are satisfies,

$$1 - 2\kappa_c = \mathcal{B}_c - \mathcal{B}_c^2 \frac{\kappa_c}{2 - 2\kappa_c}. \quad (5)$$

While this phase transition occurs in equilibrium, previous studies [27,28,37,53,54] show that its signatures can appear in nonequilibrium quantum quenches, motivating us to explore these within Liang information flow.

Since the model in Eq. (4) is nonintegrable for generic parameter values, we resort to numerical simulations [time-dependent variational principle (TDVP) and density matrix renormalization group [55]] for our results. However, we first explore the integrable limit $\kappa = 0$, before discussing the results for $\kappa > 0$.

$\kappa = 0$: For $\kappa = 0$, we apply a canonical transformation ($\sigma^x \to \sigma^z, \sigma^z \to -\sigma^x$) and a Jordan-Wigner transformation to map H_L to spinless fermions, yielding $\mathcal{B}_c = 1$ in the thermodynamic limit. The one-site density matrix required for computation is $\rho_j = [(\mathbb{I} + \langle\sigma_j^z\rangle\sigma^z)/2]$ [38]. The time evolution of $\langle\sigma^z\rangle$ can be found semianalytically due to the Hamiltonian being quadratic in fermionic operators [36].

In Fig. 3(a), we show the flow of Liang information for $d = 3$, when the initial state is the ground state at $\mathcal{B} = 0.01$ and we quench to different values of $\mathcal{B}$. When $\mathcal{B}$ is small,

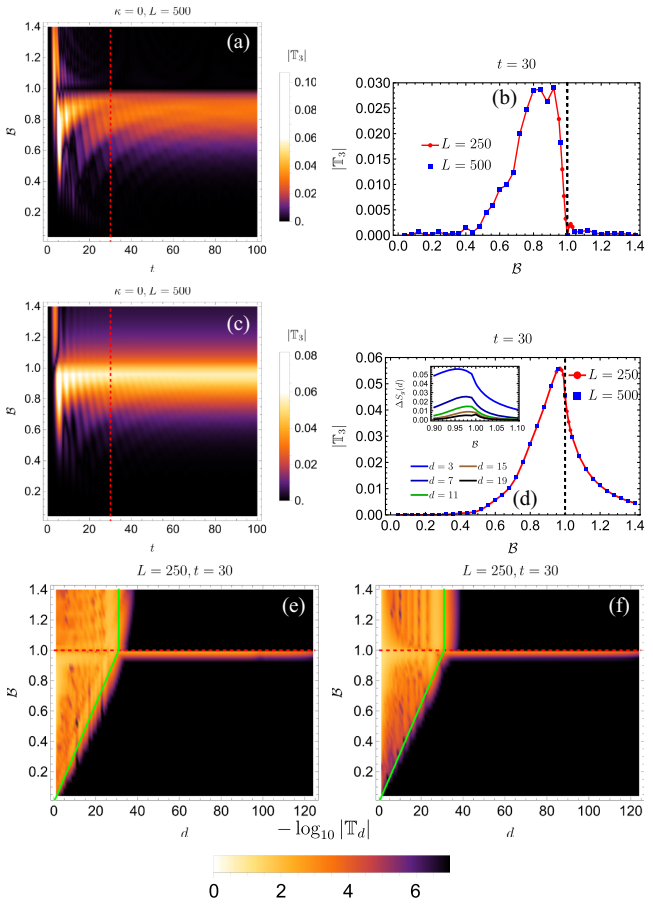

FIG. 3. Variation of cumulative Liang information flow ($|\mathbb{T}_d|$) for quenches to different $\mathcal{B}$ fields at $\kappa = 0$. (a),(b) Initial state is the ground state of $\mathcal{B} = 0.01$. (c),(d) Initial state is the ground state of the respective $\mathcal{B}$. The inset of (d) shows $\Delta S_g(d)$, the entanglement difference at distance d from the frozen site, between normal and frozen site ground states, as a function of $\mathcal{B}$. (a) $|\mathbb{T}_3|$ at three sites from the frozen site; red dashed lines mark the cross section in (b), where the black line indicates the critical point. (e),(f) Spatial profiles of Liang information flow for quenches at $L = 250$ at a chosen time. (e) follows the setup in (a) and (f) follows that in (c). The red dashed line marks $\mathcal{B}_c = 1$, and green lines show the fastest quasiparticle's reach.

the initial state in this regime has a large overlap with the ground state, thus limiting nontrivial evolution and Liang information flow. The flow gradually increases as we increase $\mathcal{B}$ toward $\mathcal{B}_c$ due to increased quantum fluctuations introduced by the σ^x in the dynamics. However, if $\mathcal{B}$ is too large (deep inside the paramagnetic phase), evolution becomes dominated by the local σ^x term and we notice the expected qualitative behavior of small Liang information flow in Fig. 3(b) for $\mathcal{B} > 1$. However, the peak of quantum causation appears to be shifted from the critical $\mathcal{B}_c = 1$, where one would expect the quantum effects in the evolution the most. One possible cause for this is our choice of initial state having significant overlaps with several high energy states in this regime. To verify this, we study another initial state: the ground state of the corresponding $\mathcal{B}$ where causality is being computed, the results of which are shown in Figs. 3(c) and 3(d), which gives us almost the expected features with the peak occurring closer to $\mathcal{B}_c$. The reason for the remaining skewness toward the ferromagnetic phase is the greater influence of nearby neighbors in the dynamics due to dominance of a nearest-neighbor term, which is seen in the maxima of $|\mathbb{T}_d|$ when $t \gg d$. The effect becomes more prominent for nonground initial states. Furthermore, from the well-known quasiparticle picture of information propagation for local quenches [39] that holds for Fig. 3(d), we deduce that, for $t \gg d$, $|\mathbb{T}_d|$ is effectively the difference of $S(\rho_A)$ for site A at a distance d from the frozen site, for the ground states of the unfrozen and frozen system. We call this quantity $\Delta S_g(d)$ and plot it in the inset to show the resemblance. As evident from the plot, this feature is prominent near the edge (small d) where the flow is strongest and is embedded in the ground state of the model. This concludes our explanation of the peak-before-criticality phenomena.

Finally, we plot the spatial profile of Liang information flow at time $t = 30$ in Figs. 3(e) and 3(f). We make two key observations in these plots. First, the causation shows a spatial envelope. This is again qualitatively consistent with the picture: quasiparticles carry information in the system [39,56]. To corroborate, we show the distance covered by the fastest quasiparticle for $t = 30$ by the green line, whose velocity is $\mathrm{Min}(1, \mathcal{B})$. The small deviations can be attributed to the choice of initial state and finite sizes. Second, regardless of the initial state chosen, there is a small but highly nonlocal causation near or at the critical point which coincides with the divergence of correlation length of the ground state. This behavior is caused by the participation of a edge localized eigenmode [57] with diverging localization length near criticality in the dynamics. This effect is beyond the quasiparticle picture, as there is no propagation of plane wave (sinusoidal) eigenmodes, yet an extended eigenstate with long-range entanglement participates in dynamics, which exerts a quantum nonlocal causation upon freezing a site. This is a rare example of beyond quasiparticle quantum nonlocal behavior in spin systems.

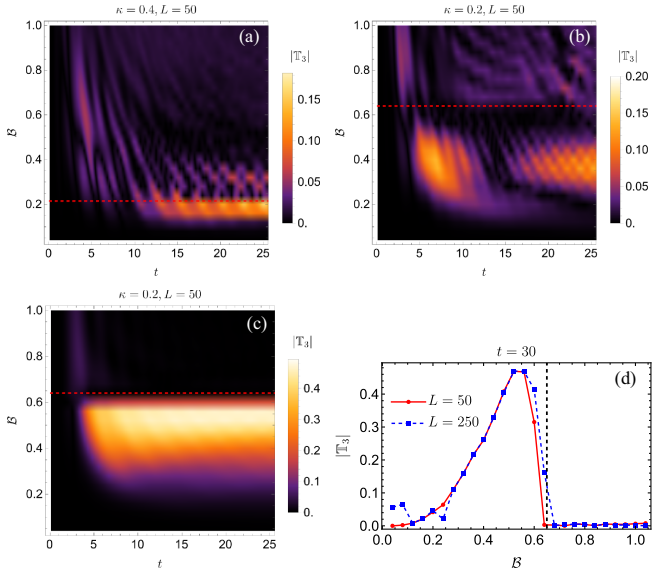

FIG. 4. Variation of absolute Liang information flow for quenches to different $\mathcal{B}$ fields at fixed $\kappa \neq 0$, computed via TDVP for system sizes $L = 50, 250$. (a) $|\mathbb{T}_3|$ at three sites from the frozen site for $\kappa = 0.4$, starting from the ferromagnetic state $|\downarrow\downarrow\cdots\downarrow\rangle$. (b) Same as (a) for $\kappa = 0.2$. (c) $|\mathbb{T}_3|$ for $\kappa = 0.2$ starting from the ground state, similar to Fig. 3(c). (d) Cross section of (c) at $t = 30$ compared with $|\mathbb{T}_3|$ for $L = 250$. Red and black dashed lines denote $\mathcal{B}_c$ from Eq. (5).

Immediately after a critical point [which can be shown to be at $\mathcal{B}_c \sim L/(L+1)$ due to the finite-size effect], this mode changes to a plane wave and the nonlocality vanishes [36].

$\kappa > 0$:For $\kappa > 0$, performing quenches in $\mathcal{B}$ or κ yields similar results [36]. In Fig. 4, we show the features shown by quantum Liang information flow for the nonintegrable interacting model. As in the previous section, we study two initial states: the ferromagnetic state $|\downarrow\downarrow\downarrow\cdots\downarrow\rangle$, which is the ground state at $\kappa = \mathcal{B} = 0$, and the ground state of $\mathcal{B}$, where information flow is computed [59].

In Fig. 4(a), despite starting from the ferromagnetic initial state with a smaller system size $L = 50$ compared to Fig. 3, we observe a peak in quantum Liang information flow very close to criticality. The proximity of the peak to the critical point compared to the $\kappa = 0$ case is due to the fact that larger κ values push the critical point toward $\mathcal{B} = 0$. Consequently, even at these system sizes, this initial state maintains sufficient overlap with the ground state of the Hamiltonian before the critical point, thereby exhibiting the expected behavior.

However, as we decrease κ to 0.2, the ferromagnetic state no longer maintains a high overlap with the ground state near the corresponding critical point. Furthermore, the system is now ergodic due to its nonintegrable nature, implying the evolution of such a state at the same timescales is no longer restricted to the low energy sector (as can be verified by, for example, growth of entanglement). However, the causation peak still necessarily exists because

quantum fluctuations have to maximize somewhere in between the extreme cases $\mathcal{B} \ll 1$ and $\mathcal{B} \gg 1$. Although, it need not bear any relation to the phase transition point; it just depends on the dynamics. This is verified in Fig. 4(b), which shows the peak much before the critical point denoted by the red dashed line.

Nonetheless, we recover the "peak near criticality" akin to the noninteracting case, once the initial state is the ground state [36], as shown in Figs. 4(c) and 4(d) for Liang information flow to nearby sites with $d = 3$. In the integrable model, starting from even nonground initial states, we can capture the same features of the ground state transition, as seen from Fig. 3(e). In contrast, in the nonintegrable case, only the low energy initial states show the correct behavior. Thus, the maximum causality depends on the competing behavior of the various Hamiltonian terms on the initial state.

Discussion—In this Letter, we have unraveled causation behavior in quantum chains using the recently formulated quantum Liang information flow. We established that causality peaks do not align with maxima in correlation, as causality is quantified by the *difference* in quantum correlations. We found a democracy of influence in the fully delocalized regime and near-site causation in the localized regime. Furthermore, diverging correlation lengths in ground state second-order phase transitions manifest as nonlocal quantum causation. We also found that the causation peak for nearby sites occurs slightly toward the ordered side of the transition, acting as a nonequilibrium herald to the equilibrium phase transition.

The quantum Liang information flow probe quantifies the influence of different couplings in a Hamiltonian to induce criticality. While classical Liang-Kleeman information has improved artificial intelligence (AI) simulations by uncovering causal relationships in data [60], our result shows that its quantum counterpart can characterize phase transitions in spin systems, and utilizing it on random graph structures can be key to leveraging quantum computation for nondeterministic-polynomial-hard problems, for example, in tackling bottlenecks of quantum annealing [61]. Causality peaks naturally delineate dominant interactions around transitions, thus offering a diagnostic tool for detecting structural traits inducing quantum phase transitions, which can be useful in optimizing schedules for critical state preparation, a challenging task. Possible additional applications include identifying resonant regions in many-body localization [62,63] and tracking participating qubits in quantum reservoir computing [64], similar to its role in improving classical AI [60]. The examples provided in this Letter can be tested in D-wave architecture, where transverse Ising models with $O(100)$ sites have been simulated [65–67], or in trapped ion systems (see Appendix B).

Acknowledgments—R. G. thanks K. Sengupta, A. Das, M. Sarkar and A. Nico-Katz for discussions. R. G. and S. B. acknowledge the UKRI EPSRC Grants "Nonergodic quantum manipulation" No. EP/R029075/1 and Many-Body Phases in Continuous-Time Quantum Computation No. EP/Y004590/1 for support. Y. B. acknowledges support from National Natural Science Foundation of China (Grant No. 12404551) and the China Postdoctoral Science Foundation (Grant No. 2024M750339).

[1] L. Amico, A. Osterloh, F. Plastina, R. Fazio, and G. Massimo Palma, Dynamics of entanglement in one-dimensional spin systems, Phys. Rev. A **69**, 022304 (2004).
[2] A. Polkovnikov, K. Sengupta, A. Silva, and M. Vengalattore, Colloquium: Nonequilibrium dynamics of closed interacting quantum systems, Rev. Mod. Phys. **83**, 863 (2011).
[3] S. Campbell, T. J. G. Apollaro, C. Di Franco, L. Banchi, A. Cuccoli, R. Vaia, F. Plastina, and M. Paternostro, Propagation of nonclassical correlations across a quantum spin chain, Phys. Rev. A **84**, 052316 (2011).
[4] T. J. G. Apollaro, S. Lorenzo, and F. Plastina, Transport of quantum correlations across a spin chain, Int. J. Mod. Phys. B **27**, 1345035 (2013).
[5] T. Boorman, M. Szyniszewski, H. Schomerus, and A. Romito, Diagnostics of entanglement dynamics in noisy and disordered spin chains via the measurement-induced steady-state entanglement transition, Phys. Rev. B **105**, 144202 (2022).
[6] A. K. Pattanayak and P. Brumer, Chaos and Lyapunov exponents in classical and quantal distribution dynamics, Phys. Rev. E **56**, 5174 (1997).
[7] A. Lakshminarayan, Entangling power of quantized chaotic systems, Phys. Rev. E **64**, 036207 (2001).
[8] J. N. Bandyopadhyay and A. Lakshminarayan, Testing statistical bounds on entanglement using quantum chaos, Phys. Rev. Lett. **89**, 060402 (2002).
[9] X. Wang, S. Ghose, B. C. Sanders, and B. Hu, Entanglement as a signature of quantum chaos, Phys. Rev. E **70**, 016217 (2004).
[10] V. Balasubramanian, P. Caputa, J. M. Magan, and Q. Wu, Quantum chaos and the complexity of spread of states, Phys. Rev. D **106**, 046007 (2022).
[11] J. Maldacena, S. H. Shenker, and D. Stanford, A bound on chaos, J. High Energy Phys. 08 (2016) 106.
[12] I. Kukuljan, S. Grozdanov, and P. Tomaž, Weak quantum chaos, Phys. Rev. B **96**, 060301(R) (2017).
[13] A. W. Harrow, L. Kong, Z.-W. Liu, S. Mehraban, and P. W. Shor, Separation of out-of-time-ordered correlation and entanglement, PRX Quantum **2**, 020339 (2021).
[14] J. Riddell and E. S. Sørensen, Out-of-time ordered correlators and entanglement growth in the random-field XX spin chain, Phys. Rev. B **99**, 054205 (2019).
[15] T. Notenson, I. García-Mata, A. J. Roncaglia, and D. A. Wisniacki, Classical approach to equilibrium of out-of-time ordered correlators in mixed systems, Phys. Rev. E **107**, 064207 (2023).
[16] T. Xu, T. Scaffidi, and X. Cao, Does scrambling equal chaos?, Phys. Rev. Lett. **124**, 140602 (2020).

[17] M. Pandey, P. W. Claeys, D. K. Campbell, A. Polkovnikov, and D. Sels, Adiabatic eigenstate deformations as a sensitive probe for quantum chaos, Phys. Rev. X **10**, 041017 (2020).

[18] C. Lim, K. Matirko, A. Polkovnikov, and M. O. Flynn, Defining classical and quantum chaos through adiabatic transformations, arXiv:2401.01927.

[19] Č. Brukner, Quantum causality, Nat. Phys. **10**, 259 (2014).

[20] X. S. Liang and R. Kleeman, Information transfer between dynamical system components, Phys. Rev. Lett. **95**, 244101 (2005).

[21] X. S. Liang, Information flow and causality as rigorous notions *ab initio*, Phys. Rev. E **94**, 052201 (2016).

[22] X. S. Liang, Causation and information flow with respect to relative entropy, Chaos **28**, 075311 (2018).

[23] B. Yi and S. Bose, Quantum Liang information flow as causation quantifier, Phys. Rev. Lett. **129**, 020501 (2022).

[24] A. Mitra, Quantum quench dynamics, Annu. Rev. Condens. Matter Phys. **9**, 245 (2018).

[25] K. Sengupta, S. Powell, and S. Sachdev, Quench dynamics across quantum critical points, Phys. Rev. A **69**, 053616 (2004).

[26] P. Basu and S. R. Das, Quantum quench across a holographic critical point, J. High Energy Phys. 01 (2012) 103.

[27] A. Haldar, K. Mallayya, M. Heyl, F. Pollmann, M. Rigol, and A. Das, Signatures of quantum phase transitions after quenches in quantum chaotic one-dimensional systems, Phys. Rev. X **11**, 031062 (2021).

[28] C. B. Dağ, P. Uhrich, Y. Wang, I. P. McCulloch, and J. C. Halimeh, Detecting quantum phase transitions in the quasistationary regime of Ising chains, Phys. Rev. B **107**, 094432 (2023).

[29] H. Shen, P. Zhang, R. Fan, and H. Zhai, Out-of-time-order correlation at a quantum phase transition, Phys. Rev. B **96**, 054503 (2017).

[30] Z.-H. Sun, J.-Q. Cai, Q.-C. Tang, Y. Hu, and H. Fan, Out-of-time-order correlators and quantum phase transitions in the Rabi and Dicke models, Annalen Phys. **532**, 1900270 (2020).

[31] M. Heyl, F. Pollmann, and B. Dóra, Detecting equilibrium and dynamical quantum phase transitions in ising chains via out-of-time-ordered correlators, Phys. Rev. Lett. **121**, 016801 (2018).

[32] T. Fukuhara, A. Kantian, M. Endres, M. Cheneau, P. Schauß, S. Hild, D. Bellem, U. Schollwöck, T. Giamarchi, C. Gross, I. Bloch, and S. Kuhr, Quantum dynamics of a mobile spin impurity, Nat. Phys. **9**, 235 (2013).

[33] E. J. Torres-Herrera and L. F. Santos, Local quenches with global effects in interacting quantum systems, Phys. Rev. E **89**, 062110 (2014).

[34] M. Kohmoto, Metal-insulator transition and scaling for incommensurate systems, Phys. Rev. Lett. **51**, 1198 (1983).

[35] S. Aubry and G. André, Analyticity breaking and anderson localization in incommensurate lattices, Ann. Israel Phys. Soc **3**, 18 (1980).

[36] See Supplemental Material at http://link.aps.org/supplemental/10.1103/PhysRevLett.134.150202 for other parameter results and details of analytical computations, which includes Refs. [37–45].

[37] J. H. Robertson, R. Senese, and F. H. L. Essler, A simple theory for quantum quenches in the ANNNI model, SciPost Phys. **15**, 032 (2023).

[38] T. J. Osborne and M. A. Nielsen, Entanglement in a simple quantum phase transition, Phys. Rev. A **66**, 032110 (2002).

[39] P. Calabrese and J. Cardy, Entanglement and correlation functions following a local quench: A conformal field theory approach, J. Stat. Mech. (2007) P10004.

[40] R. Ghosh and A. Das, Disorder-induced enhancement of entanglement growth in one dimension: Information leakage at the scale of the localization length, Phys. Rev. B **103**, 024202 (2021).

[41] I. Peschel, Calculation of reduced density matrices from correlation functions, J. Phys. A **36**, L205 (2003).

[42] I. Peschel and V. Eisler, Reduced density matrices and entanglement entropy in free lattice models, J. Phys. A **42**, 504003 (2009).

[43] E. Lieb, T. Schultz, and D. Mattis, Two soluble models of an antiferromagnetic chain, Ann. Phys. (N.Y.) **16**, 407 (1961).

[44] I. Affleck and A. W. W. Ludwig, Universal noninteger "ground-state degeneracy" in critical quantum systems, Phys. Rev. Lett. **67**, 161 (1991).

[45] H. Rieger and F. Iglói, Semiclassical theory for quantum quenches in finite transverse Ising chains, Phys. Rev. B **84**, 165117 (2011).

[46] W. Selke, The ANNNI model—theoretical analysis and experimental application, Phys. Rep. **170**, 213 (1988).

[47] A. K. Chandra and S. Dasgupta, Floating phase in the one-dimensional transverse axial next-nearest-neighbor Ising model, Phys. Rev. E **75**, 021105 (2007).

[48] S. Suzuki, J.-i. Inoue, and B. K. Chakrabarti, ANNNI model in transverse field, in *Quantum Ising Phases and Transitions in Transverse Ising Models* (Springer, Berlin, Heidelberg, 2013), pp. 73–103.

[49] D. Allen, P. Azaria, and P. Lecheminant, A two-leg quantum Ising ladder: A bosonization study of the ANNNI model, J. Phys. A **34**, L305 (2001).

[50] A. Nagy, Exploring phase transitions by finite-entanglement scaling of MPS in the 1D ANNNI model, New J. Phys. **13**, 023015 (2011).

[51] P. R. C. Guimarães, J. a. A. Plascak, F. C. Sá Barreto, and J. a. Florencio, Quantum phase transitions in the one-dimensional transverse Ising model with second-neighbor interactions, Phys. Rev. B **66**, 064413 (2002).

[52] M. Beccaria, M. Campostrini, and A. Feo, Density-matrix renormalization-group study of the disorder line in the quantum axial next-nearest-neighbor Ising model, Phys. Rev. B **73**, 052402 (2006).

[53] C. B. Dağ, Y. Wang, P. Uhrich, X. Na, and J. C. Halimeh, Critical slowing down in sudden quench dynamics, Phys. Rev. B **107**, L121113 (2023).

[54] P. Zanardi and N. Paunković, Ground state overlap and quantum phase transitions, Phys. Rev. E **74**, 031123 (2006).

[55] M. Fishman, S. R. White, and E. M. Stoudenmire, Codebase release 0.3 for ITensor, SciPost Phys. Codebases, 10.21468/SciPostPhysCodeb.4-r0.3 (2022).

[56] P. Ruggiero, P. Calabrese, L. Foini, and T. Giamarchi, Quenches in initially coupled Tomonaga-Luttinger liquids: A conformal field theory approach, SciPost Phys. **11**, 055 (2021).

[57] Ferromagnetic phase of $\kappa = 0$ for OBC hosts this mode, see Ref. [58] and Supplemental Material [36].

[58] M. Kormos, Inhomogeneous quenches in the transverse field Ising chain: Scaling and front dynamics, SciPost Phys. **3**, 020 (2017).
[59] A tiny longitudinal field $O(10^{-4})$ is added to prevent degeneracy for small $\mathcal{B}$.
[60] M. Tyrovolas, X. S. Liang, and C. Stylios, Information flow-based fuzzy cognitive maps with enhanced interpretability, Granular Comput. **8**, 2021 (2023).
[61] T. Albash and D. A. Lidar, Adiabatic quantum computation, Rev. Mod. Phys. **90**, 015002 (2018).
[62] R. Ghosh and M. Žnidarič, Resonance-induced growth of number entropy in strongly disordered systems, Phys. Rev. B **105**, 144203 (2022).
[63] A. Morningstar, L. Colmenarez, V. Khemani, D. J. Luitz, and D. A. Huse, Avalanches and many-body resonances in many-body localized systems, Phys. Rev. B **105**, 174205 (2022).
[64] J. Dudas, B. Carles, E. Plouet, F. A. Mizrahi, J. Grollier, and D. Marković, Quantum reservoir computing implementation on coherently coupled quantum oscillators, npj Quantum Inf. **9**, 64 (2023).
[65] Y. Bando, Y. Susa, H. Oshiyama, N. Shibata, M. Ohzeki, F. J. Gómez-Ruiz, D. A. Lidar, S. Suzuki, A. del Campo, and H. Nishimori, Probing the universality of topological defect formation in a quantum annealer: Kibble-zurek mechanism and beyond, Phys. Rev. Res. **2**, 033369 (2020).
[66] A. D. King *et al.*, Quantum critical dynamics in a 5,000-qubit programmable spin glass, Nature (London) **617**, 61 (2023).
[67] J. Vodeb, J.-Y. Desaules, A. Hallam, A. Rava, G. Humar, D. Willsch, F. Jin, M. Willsch, K. Michielsen, and Z. Papić, Stirring the false vacuum via interacting quantized bubbles on a 5564-qubit quantum annealer, Nat. Phys. **21**, 386 (2025).
[68] D. F. V. James, P. G. Kwiat, W. J. Munro, and A. G. White, Measurement of qubits, Phys. Rev. A **64**, 052312 (2001).

Correction: An affiliation indicator was erroneously included with the first author's name during the proof process and has been removed.

End Matter

Appendix A: Further details about the setup—In the top three chains of Fig. 1, we depict situations with only nearest-neighbor couplings. In this scenario, removing a site results in a break in the chain, and the effective evolution then occurs within a smaller chain, and the difference of $S(\rho)$ at the target site between the normal and smaller chain gives the Liang information flow. With longer-range couplings, as the next-nearest-neighbor case shown in the lower half of Fig. 1, freezing one site does not break the chain, positioning the target site consistently within the bulk. However, we must emphasize that, while computing causation, the breakage of a chain is not a source of any issues. Just to complete this discussion, we would like to mention that to prevent chain breakage upon freezing site p, one must ensure couplings of range $p+1$ in a chain with open boundary conditions. Furthermore, for periodic boundary conditions, there is a connection between sites 1 and L, preventing chain breakage, but transforming the system into an open boundary condition system upon freezing a site. However, we opt for open boundary conditions in this Letter to avoid this additional complexity. Although it should not significantly differ from the results in this Letter for unitary evolution, discrepancies may arise in the nonunitary scenario, particularly where potential skin effects emerge, and for topological phase transitions. We plan to explore these differences in a subsequent study.

Appendix B: Experimental protocol—To compute the Liang information flow to a specific distance, one needs to follow a two-step procedure: (1) To obtain the results when starting from the ground state of the Ising model, one needs to first initialize the model in its ground state and then select any site, preferably away from the edges of the chain. One then needs to perform single-site tomography to obtain information about the reduced density matrix of the problem. For the integrable transverse Ising chain, this reduces to σ^z measurements at the specific site. On the other hand, to obtain the results starting from the ferromagnetic initial state, one

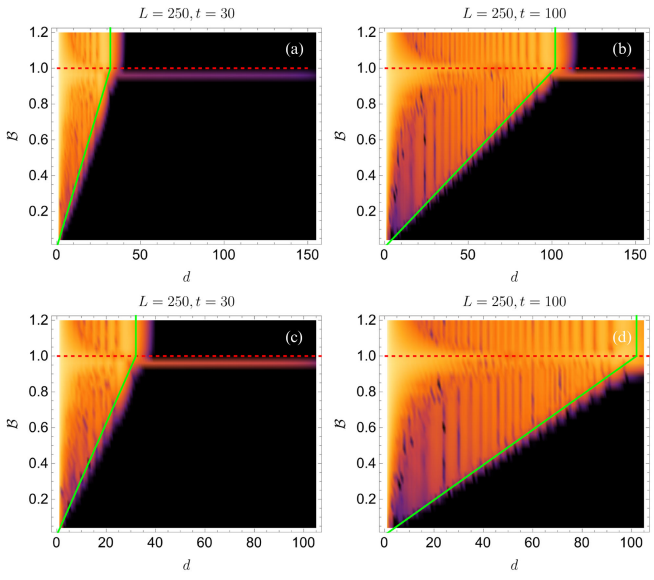

FIG. 5. (a),(b) The spatial profile for Liang information flow for $t = 30$ and $t = 100$, respectively, when site $L/2 - 30$ is frozen for $L = 250$. (c),(d) The corresponding plots when site $L/2 + 20$ is frozen. There is no qualitative difference in the results. Note that the points on the y axis are taken 0.04 apart; hence the small gap between the dashed lines, which denote $\mathcal{B}_c = 1$, and the point of beyond quasiparticle quantum nonlocality.

needs to initialize the system in this state and allow it to evolve under the corresponding Hamiltonians for time t. Then, one needs to perform single-site tomographic measurements to obtain the reduced density matrix and thus the von Neumann entropy. Note that the reduced density matrix for any general nonintegrable for a single site can be reconstructed by three Pauli measurements using the Stokes parameters [68], which can be the protocol for tomography here. (2) In the second step, one needs to reinitialize the system to either the ground state of the same Hamiltonian as the previous step or the ferromagnetic initial state, depending on which result one intends to obtain. Then, according to the required distance d, one should suddenly decouple the site (by turning off the relevant couplings or applying a large local magnetic field) at a distance d from the previously measured site and allow the system to evolve freely. Again, one needs to perform tomographic measurements on the same site as before, after the same time t. This would give us the entropy with a site frozen. The difference between these two values yields the Liang information.

It should be noted that freezing the middle site was simply a choice made for numerical simulations; freezing any other site would yield qualitatively similar results. This implies that, to obtain the plot showing results for different distances, one does not need to repeat step (1) for each distance. Instead, one can repeat step (2) by decoupling different sites at varying distances each time to obtain the variation of Liang information with distance. This is verified in Fig. 5, showing that similar qualitative results can be achieved by keeping the target site fixed and varying the position of the frozen site, which is operationally simpler.